

Accepted Manuscript

Title: A magnetically recoverable nanocatalyst based on functionalized mesoporous silica

Author: Piyali Bhanja Tapas Sen Asim Bhaumik

PII: S1381-1169(16)30020-6
DOI: <http://dx.doi.org/doi:10.1016/j.molcata.2016.01.020>
Reference: MOLCAA 9752

To appear in: *Journal of Molecular Catalysis A: Chemical*

Received date: 11-11-2015
Revised date: 24-12-2015
Accepted date: 19-1-2016



Please cite this article as: Piyali Bhanja, Tapas Sen, Asim Bhaumik, A magnetically recoverable nanocatalyst based on functionalized mesoporous silica, *Journal of Molecular Catalysis A: Chemical* <http://dx.doi.org/10.1016/j.molcata.2016.01.020>

This is a PDF file of an unedited manuscript that has been accepted for publication. As a service to our customers we are providing this early version of the manuscript. The manuscript will undergo copyediting, typesetting, and review of the resulting proof before it is published in its final form. Please note that during the production process errors may be discovered which could affect the content, and all legal disclaimers that apply to the journal pertain.

A magnetically recoverable nanocatalyst based on functionalized mesoporous silica

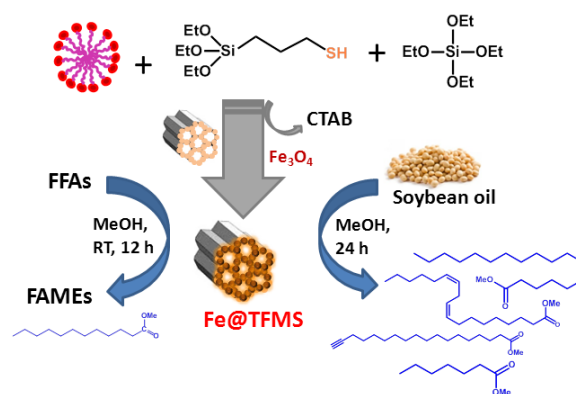
Piyali Bhanja^a, Tapas Sen^b, Asim Bhaumik^{a*} msab@iacs.res.in

^aDepartment of Materials Science, Indian Association for the Cultivation of Science, Jadavpur, Kolkata–700 032, India.

^bNanobiomaterials Research Group, Centre for Materials Science, School of Physical Sciences and Computing, University of Central Lancashire, Preston, PR1 2HE, UK.

*Corresponding author.

Graphical Abstract



Highlights

- Synthesis of a 2D-hexagonally ordered thiol functionalized mesoporous silica.
- Magnetically recoverable nanocatalyst with high BET surface area.
- Esterification/transesterification for the synthesis of biodiesels at room temperature.
- Lewis acidity of the grafted Fe₃O₄ nanoparticles

Abstract

A magnetically separable 2D-hexagonally ordered thiol functionalized mesoporous silica material (Fe@TFMS) has been synthesized through co-condensation reaction of 3-mercaptopropyltriethoxysilane (MPTES) and tetraethylorthosilicate (TEOS) using cetyltrimethylammonium bromide (CTAB) as a cationic surfactant followed by immobilization of Fe₃O₄ nanocrystallites at the functionalized mesopore surface. Powder X-ray diffraction (XRD), N₂ adsorption/desorption analysis, FT-IR, TEM, FE-SEM, TGA/DTA, XPS and NH₃-TPD tools are employed to characterize the materials. This functionalized mesoporous material exhibited high catalytic activity in the biodiesel production from a wide range of long chain fatty acids and soybean oil. The material showed high Lewis acidity of 1.02 mmol g⁻¹ with a good Brunauer-Emmett-Teller (BET) surface area of 411 m² g⁻¹. Fe@TFMS showed excellent catalytic efficiency for this esterification reaction using methanol as a solvent cum reactant under eco-friendly and mild reaction conditions (room temperature, 25 °C).

Keywords: Functionalized mesoporous material; superparamagnetic material; bio-diesel production; Lewis acidity; eco-friendly conditions.

1. Introduction

In recent years biodiesel synthesis has attracted widespread interest in the context of future energy demand. Limited reserve of our natural fossil fuels, environmental degradation as a result of green-house gas emission from the burning of fossil fuels and other organic resources has prompted the demand of biodiesels [1]. Biodiesel is produced from the long chain fatty acids (animal fat and vegetable oil) through the esterification reaction with methanol/ethanol [2] and these compounds have huge potential as alternative resource to fossil fuels. The vegetable oil [3-5] and animal fats [6,7] are currently considered as the most attractive and easily available feedstocks for biodiesel production due to their lower market value in comparison with virgin oils. It is a sustainable, biodegradable, does not emit any hazardous and toxic compounds (green energy), suitable for use in the actual compression and ignition engine without any major purification, which could be produced very easily through acid or base-catalyzed esterification and transesterification reactions [8,9]. Various strategies have been employed to overcome the common problems faced in the synthesis of biodiesels. Several insoluble solid acid catalysts like cation-exchange resin [10], combination of cation-anion exchange resin [11], phase transfer catalyst [12], mixed oxides [13], functionalized mesoporous silica [14], mesoporous carbon [15] and enzyme-immobilised magnetic support [16] etc. are utilized for the esterification reactions, substituting the homogeneous inorganic acid catalysts. However, efficiencies of many of the heterogeneous acid catalysts are quite unsatisfactory. For example zeolites showed poor catalytic efficiency due to the low densities and low accessibility of the acidic sites [17,18], whereas sulfated zirconia [19,20] does not have high BET surface area. Besides, these catalysts require high temperature reactivation. Further, diarryl ammonium incorporated catalyst support [21] although showed good catalytic activity it needs the use of expensive triflic acid, high temperature and pressure for the synthesis.

To fabricate a solid Lewis acid catalyst having good BET surface area substantial efforts has been devoted, but there are some intrinsic problems due to less accessibility of the active sites and enhanced diffusion limitation of reactant resulting in less catalytic activity and poor selectivity of the product. In recent years, the solid porous materials have been employed for biodiesel synthesis such as organically functionalized mesoporous silica material [22-24], metal organic frameworks (MOF) [25-27] and acid functionalized ionic liquids [28-30] etc. In most of the cases biodiesel is synthesized under drastic conditions [31], which is not eco-friendly. For the production of biofuel green synthetic pathways [32] are highly desirable to avoid those drastic conditions. There are only few reports for the biodiesel production at room temperature [33,34], though the main drawback of this reaction is the reversibility of the esterification reaction. Although Tang et al have reported the Ca/Al/Fe₃O₄ magnetic composite as solid catalyst in the transesterification reaction [35] but the material has very poor BET surface area. On the other hand the magnetically recyclable ionic liquid immobilized mesoporous material FSS-IL can be used as an efficient catalyst for the esterification of oleic acid with ethanol for high biodiesel yield of 93.5% [36], but it requires elevated temperature for the reaction. During esterification reaction the product esters could be easily hydrolyzed in the presence of water molecule. To overcome this problem we have design a magnetically separable mesoporous heterogeneous catalyst, which can easily accommodate the water molecule from the reaction mixture, facilitating the esterification reaction at room temperature in the presence of minimum amount of methanol as a reagent and solvent.

Herein we report the synthesis of magnetically recoverable superparamagnetic Fe₃O₄ nanoparticle immobilized functionalized mesoporous silica having considerably high surface area with a tunable porosity and it displays excellent catalytic activity in the bio-diesel

production at room temperature. Thiol functionalized mesoporous MCM-41 is prepared using 3-mercaptopropyltrimethoxysilane via co-condensation reaction. The reaction between thiol functionalized MCM-41 and dispersed Fe_3O_4 in absolute ethanol medium offers the formation of magnetically separable mesoporous material Fe@TFMS. The material has been characterized through PXRD, N_2 sorption, FESEM, XPS, FTIR spectroscopic tools, and displayed very easy product/catalyst recovery and good recycling efficiency without any loss of catalytic activity after five reaction cycles suggesting its future potential in large scale biodiesel production.

2. Experimental Section

2.1. Chemicals

Cetyltrimethylammonium bromide (CTAB), tetraethyl orthosilicate (TEOS) and 3-mercaptopropyltriethoxysilane (MPTES, $M_{\text{wt}} = 196.34$ g/mol) were purchased from Sigma Aldrich. Anhydrous ferrous chloride ($M_{\text{wt}} = 126.75$ g/mol) and ferric chloride ($M_{\text{wt}} = 162.20$ g/mol) was purchased from Merck, India. The solvents were used as received without further purification.

2.2. In-situ synthesis of thiol functionalized mesoporous silica (TFMS)

In a 100 ml cleaned plastic beaker 0.006 M (2.42 g) of CTAB was dissolved in 20 mL distilled water. This is followed by the addition of 0.02 M (4.166 g) tetraethylorthosilicate (TEOS) and 0.005 M (0.981 g) MPTES. The resulting white gel was allowed to stir for 15 min and then aqueous solution of NaOH was added dropwise to maintain the alkaline pH (11.7) conditions. The slurry was kept under static condition in polypropylene bottle at 75 °C temperature for 3 days. After the thermal treatment the white solid product was washed thoroughly with distilled water to get rid of extra template molecules (CTAB) and dried in air for 24 h. Then 0.5 g of as-synthesized solid product was subjected for acid-ethanol extraction

to remove the template using 0.5 g of 1N HCl and 20 mL absolute ethanol solution mixture for two times in each batch. Finally, the extracted solid product was filtered by simple filtration technique and washed with distilled water for several times.

2.3. Synthesis of Fe_3O_4 nanoparticles

2.86 g (0.017 mol) of anhydrous $FeCl_3$ and 1.057 g (0.008 mol) of anhydrous $FeCl_2$ was dissolved in 60 mL distilled water taken in a 50 mL round bottom flask under inert atmospheric conditions. Then the reaction mixture was allowed to keep in a pre-heated oil bath at 80-85 °C temperature for 2 h after drop wise addition of aqueous ammonia (25 %) to it. The resulting black precipitate was collected through filtration and washed with distilled water for several times to neutralize it. The black coloured solid product was dried in oven at 75 °C temperature for about 2 h.

2.4. Synthesis of Fe_3O_4 immobilized thiol functionalized mesoporous silica ($Fe@TFMS$)

The thiol functionalized MCM-41 was dispersed into a cleaned 100 mL glass beaker containing 25 mL absolute ethanol. Then, the brown coloured ethanolic suspension of Fe_3O_4 (0.1 g in 100 mL distilled water) was added drop by drop to the former solution and the solution mixture was stirred continuously for 12 h at room temperature. The resulting dark brown coloured solid product was filtered, washed thoroughly with ethanol and dried in air for overnight. The schematic representation for the formation of Fe_3O_4 nanoparticle grafted thiol-functionalized MCM-41 material ($Fe@TFMS$) is shown in Scheme 1 step by step. Here the thiol functionalized MCM-41 material (TFMS) has been synthesized by co-condensation of organosilanes in the presence of CTAB under hydrothermal conditions. This is followed by the removal of the template and impregnation of Fe_3O_4 NPs at the surface of TFMS to obtain magnetic nanocatalyst $Fe@TFMS$.

3. Characterization techniques

Nitrogen adsorption/desorption isotherms were obtained by using a Quantachrome Autosorb 1-C surface area analyzer at 77 K. Prior to gas adsorption, samples were degassed for 10-12 h at 453 K under high vacuum analysis. NLDFT theory was employed for pore size distributions measurement from the nitrogen sorption isotherm using the oxygen/cylindrical pore model. The powder X-ray diffraction patterns were recorded using Bruker D8 Advance SWAX diffractometer operated at voltage of 40 kV and current 40 mA. The instrument was calibrated with a standard silicon sample, using Ni-filtered Cu K α ($\lambda=0.15406$ nm) radiation. FT-IR spectra of the functionalized mesoporous samples were recorded using a Perkin-Elmer spectrum 100 spectrophotometer. To analyze the morphology and particle size of the samples JEOL JEM 6700 field emission scanning electron microscope (FE SEM) was used. Transmission electron microscopic (TEM) images of the material were obtained using a JEOL JEM 2010 transmission electron microscope operating at 200 kV. Thermogravimetric analysis (TGA) and differential thermal analysis (DTA) of the sample were performed in a TGA instrument thermal analyzer TA-SDT Q-600 under air flow. The carbon, hydrogen, nitrogen and sulfur (CHNS) contents were determined in a Vario EL III elemental analysis analyzer. The temperature-programmed desorption of ammonia (NH₃-TPD) experiment was carried out on flow apparatus (Micrometrics TP-5080). The saturation magnetisation and magnetisation curve measurements were carried out using a 6 kOe vibrating sample magnetometer (VSM) at room temperature (RT).

4. Results and Discussions

4.1. Mesophase and nanostructure

The small angle X-ray diffraction patterns of pure MCM-41 (a), thiol functionalized mesoporous silica (b) and Fe₃O₄ nanoparticle immobilized functionalized mesoporous

material (Fe@TFMS) (c) are shown in Figure 1. As seen from the figure, each sample shows the characteristic peaks in the region of 2 to 6 degrees of 2θ , is attributed to three distinct planes 100 (strong), 110 (weak), 200 (weak), representing the ordered 2D hexagonal mesoporous materials [37-39]. The strong peaks were observed at 2θ value of 2.35° and 2.37° for thiol functionalized mesoporous silica (TFMS) and Fe_3O_4 nanoparticle immobilized mesoporous silica (Fe@TFMS), respectively. The decrease in d -spacing of 0.02 nm (from 3.75 nm to 3.72 nm) and small shift of peak position towards higher 2θ value suggested contraction of the unit cell during the immobilization of Fe_3O_4 nanoparticles at the surface of the thiol functionalized silica framework. On the other hand, the wide angle XRD pattern of Fe@TFMS is shown in Figure 2. As seen from the figure, there are several sharp peaks which match well with the Fe_3O_4 nanocrystalline phases, suggesting the crystalline nature of the material. So, the wide angle pattern of Fe_3O_4 immobilized thiol functionalized material resembled nicely with that of pure Fe_3O_4 nanocrystals [40].

4.2. Surface area and porosity of Fe@TFMS

The nitrogen adsorption/desorption isotherm of Fe@TFMS is shown in Figure 3, which displayed the typical type IV isotherm corresponding to that of the mesoporous materials together with a steep capillary raise [38-40]. The BET (Brunauer-Emmett-Teller) surface area of (Fe@TFMS) material is $411 \text{ m}^2\text{g}^{-1}$ and corresponding pore volume is 0.1858 ccg^{-1} which confirms that the synthesized Fe_3O_4 nanoparticles do not block the pores of TFMS but the surface of TFMS material will be partially covered. Employing Non Local Density Functional Theory (NLDFT) on the N_2 sorption data points the pore size distribution plot has been obtained and this is shown in the inset of Figure 3. The one sharp peak at 2.5 nm is observed in the pore size distribution plot of Fe@TFMS, suggesting the mesoporous

nature of the material. Decrease in surface area and average pore width from the conventional MCM-41 material [41] suggested stepwise functionalization at the pore surface.

4.3. Spectroscopic studies

The FTIR spectra of (a) Fe@TFMS and (b) TFMS materials are shown in Figure 4. The broad band at around 3420 cm^{-1} , is attributed to the $-\text{OH}$ stretching vibration of the adsorbed water molecules. The two absorption bands at 1094 cm^{-1} and 950 cm^{-1} are assigned to the Si-O and Si-OH vibrations, respectively in both cases. The distinct band is observed at 583 cm^{-1} in Figure 4a, can be attributed to the Fe-O spinel structure.

4.4. Thermal stability

In order to understand the thermal stability of Fe@TFMS material, TGA/DTA analysis has been carried out under air flow at $10\text{ }^\circ\text{C}$ per minute temperature ramp. As seen from the Figure 5, the first weight loss up to $95\text{ }^\circ\text{C}$, is attributed to evaporation of physically adsorbed water molecule on the material surface. The second weight loss from $207\text{ }^\circ\text{C}$ to $290\text{ }^\circ\text{C}$ could be assigned due to the decomposition of thiol functional groups. Further, from TGA data it is noticed that the sample continued to lose weight after $300\text{ }^\circ\text{C}$ due to decomposition of organic fractions (cleavage of C-C and C-Si bonds) of Fe@TFMS as well as collapse of the mesophase. So the thermal analysis data suggests that the material has considerably good thermal stability upto $207\text{ }^\circ\text{C}$. The CHNS analysis data reveals the elemental composition of Fe@TFMS material as: carbon = 14.2%, hydrogen = 4.1%, nitrogen = 0% and sulfur = 5.2%, whereas the atomic adsorption spectroscopic (AAS) analysis data suggested 1.9 wt% Fe in Fe@TFMS.

4.5. Magnetic behaviour

We have measured the low temperature magnetic moment of Fe@TFMS nanocomposite and the results are shown in Figure 6. The observed saturation magnetization of Fe@TFMS nanocomposite is around 17.6 emu/g with zero remittance, when the magnetic field is zero. This is a clear indication of superparamagnetic nature of the composite nanomaterial. In addition, the nanocomposite didn't exhibit any hysteresis, suggesting that the material is superparamagnetic in nature. The saturation magnetization of pure magnetite is reported to be around 80 emu/g. However, we have previously reported [42,43] that the saturation magnetization value could be in the order of 15 to 40 emu/g due to the presence of diamagnetic mesoporous silica framework functionalized with organic mercaptopropyl group, which could be in the case of Fe@TFMS.

4.6. X-ray photoelectron spectroscopy

To understand the electronic state of the metal ions present in Fe@TFMS, the X-ray photoelectron spectroscopy (XPS) is often employed as a versatile surface analysis technique. The XPS spectra of the Fe@TFMS material are shown in Figure 7. As seen from the figure, the binding energy peaks are appeared at 44.0 eV due to Fe 3p (Figure 7a) and 706.4 and 729.9 eV, corresponding to the spin orbit splitting components of Fe 2p_{3/2} and Fe 2p_{1/2} (Figure 7b). It is already reported that Fe 2p_{3/2} does not have any satellite peak [44] for Fe₃O₄ which is also absent in Figure 7b. Figure 7a represents the XPS spectrum of Fe 3p. On the other hand the entire XPS profile for Fe 2p could be divided into two components: Fe 2p_{1/2} and Fe 2p_{3/2}, where the ratio of Fe⁺² to Fe⁺³ is 1:2 in Fe₃O₄ as the stoichiometric balance can be expressed by the ratio of FeO and Fe₂O₃. The full scan of the XPS spectrum has been demonstrated in Figure 8 which confirms the presence of other elements (C, O, Si, S) in the mesoporous nanocomposite material. Further, presence of S2p_{1/2}/2p_{3/2} peaks at 174.0 and

S_{2s}_{1/2} peak at 231.9 eV suggested the -SH group has not been oxidized to -SO₃H group (otherwise peak at 169-170 eV would appear) which is shown in Figure 7c and 7d [45].

4.7. Surface acidity measurement

To measure the Lewis acidity of the Fe@TFMS material, temperature programmed desorption (TPD) analysis has been carried out in the temperature range of 25 to 600 °C. The material is taken in an U-type glass cell and after completion of sample outgassing, helium gas was purged through the sample for about 15 min to cool down at room temperature. For saturation purpose NH₃ gas was allowed to flow at 30ml/ min for 40 min and again helium gas was purged for 30 min through the cell to flush out the excess amount of NH₃. The NH₃-TPD desorption profile of the sample was acquired using a thermal conductivity detector (TCD) by raising the temperature at a ramp of 5 °C per minute. In Figure 9 NH₃-TPD profile of Fe@TFMS is plotted. As seen from this TPD profile that there are two peaks centred at 60 and 240 °C. These peaks could be assigned to the existence of weak to medium strength Lewis acidic sites [46] in Fe@TFMS. Total acidity corresponding to these NH₃ desorption estimated as 1.02 mmol g⁻¹. This acidity is considerably good and this has motivated us to explore the potential of Fe@TFMS in esterification and transesterification reactions over long chain fatty acids.

4.8. Electron microscopic analysis

. The solid Fe₃O₄ nanoparticles have been characterized through electron microscopic analysis to investigate the particle size, morphological features and particle size distributions. The TEM images of Fe₃O₄ nanoparticles itself are shown in the Figures 10a and 10b, which revealed the size of the Fe₃O₄ NPs of approximately 12-20 nm with a nanosphere like morphology. The transmission electron microscopic images of Fe@TFMS material are shown in Figure 10c and 10d indicating the ordered mesoporous structure with periodic

arrangement of pores of dimension of *ca.* 2.1 nm. Further, the FFT pattern of the material is shown in the inset of Figure 10e. The black coloured spot throughout the specimen indicates the presence of superparamagnetic Fe₃O₄ nanoparticle in the framework. The selected area electron diffraction (SAED) pattern of the Fe@TFMS is demonstrated in Figure 10f. On the other hand Figure 10a and 10b represents the TEM images of Fe₃O₄ nanoparticles itself. To know the morphology of the material, the field emission scanning electron microscopy (FE-SEM) analysis has been carried out. The SEM image of the Fe₃O₄ immobilized functional mesoporous material is shown in Figure 11, suggesting the Fe@TFMS material is composed of very tiny spherical nanoparticle having an average dimension of *ca.* 47.0 nm. As seen from this figure that the Fe@TFMS material is composed of uniformly distributed nanoparticles ranged throughout the whole specimen.

4.9. Catalysis

We have taken various types of long chain mono and bi-carboxylic acid as substrate for the esterification reaction using methanol as solvent cum reactant. The product was characterized through ¹H NMR and ¹³C NMR. The yields are calculated by taking total weight after proper drying it. In absence of any acid catalyst, the yield of esterification product is very low (Table 1, 7%) where lauric acid is used as a model substrate. Generally fatty acids are esterified in the presence of sulphuric acid as a homogeneous catalyst or sulfonated solid acid catalysts at high temperature [47]. There is always a big challenge to separate the catalyst from the reaction mixture in an easy way. Here our magnetically separable heterogeneous acid catalyst could be very handy. As seen from the table 1, Fe@TFMS material is more efficient for methyl ester production at room temperature using methanol as reagent and solvent.

To understand the crucial role of methanol in esterification as well as transesterification reactions, we have performed the controlled reaction at room temperature for two times where lauric acid is used as a model substrate. Furthermore, it is pertinent to mention that for esterification reaction we have used little bit excess amount of methanol. At first, the ratio of long chain mono carboxylic fatty acid and methanol was maintained in a stoichiometric ratio i.e 1:2 and resulting yield was estimated to be 76 mol%. However, when we controlled the acid–methanol ratio (1:10), the product yield was increased up to 97 mol% for the same representative substrate. In this context, Lin et al have reported the hollow Fe/CASO₃H fibre as a catalyst for biodiesel production with 80% conversion of oleic acid [48]. Thus, our Fe@TFMS catalyst is very efficient over the related iron-containing catalysts. We have also carried out the transesterification reaction of soybean oil with methanol (oil:MeOH=1:100) at room temperature and the resulting product yield was 62 %. Another problem usually faced in this reaction is that after completion of reaction, the solution mixture contains more amount of methyl ester product, very little amount of free fatty acid, solid acid catalyst and methanol. Thus, after removal of solid acid catalyst magnetically, chloroform was used for extraction purpose and the organic layer need to be washed for three times with sodium bi-carbonate solution. The product is collected after vacuum evaporation of solvent using rotary evaporator. Since, the boiling point of methanol is not very high thus it is not convenient to maintain the stoichiometric ratio. The purification of the methyl ester product is much easier in the presence of excess amount of methanol, which can act as reagent and solvent. We have proposed a mechanism for this esterification reaction catalyzed by Fe@TFMS and this is shown in Scheme 2. Highly Lewis acidic Fe⁺³ sites present in the Fe₃O₄ NPs of the Fe@TFMS catalyst is responsible for this acid catalyzed transesterification reaction [49]. At first protonation/electron donation to Fe³⁺ sites of the acidic sites of the catalyst with the carbonyl oxygen increase the electrophilicity of carbonyl carbon. Then the

reaction undergoes 1,2 addition of alcohol followed by proton transfer to one of the –OH group. Subsequently, the water elimination leads to the formation of esterified product.

^1H and ^{13}C NMR chemical shifts of various long chain fatty acid methyl esterified product are given (the respective spectra are shown in ESI)

$\text{CH}_3\text{-(CH}_2\text{)}_{10}\text{-COOMe}$: ^1H NMR (500 MHz, CDCl_3) $\delta = 3.62$ (3H, s); $\delta = 2.25\text{--}2.30$ (2H, t); $\delta = 1.59$ (2H, m); $\delta = 1.35$ (16H, m); $\delta = 0.84$ (3H, m); ^{13}C NMR (125 MHz, CDCl_3) $\delta = 175.1$; 51.3; 34.2; 32.1; 29.6; 29.5; 29.4; 29.3; 29.2; 25.1; 22.7; 14.2.

$\text{CH}_3\text{-(CH}_2\text{)}_{12}\text{-COOMe}$: ^1H NMR (500 MHz, CDCl_3) $\delta = 3.63$ (3H, s); $\delta = 2.28$ (2H, t); $\delta = 1.50$ (2H, m); $\delta = 1.25$ (20H, m); $\delta = 0.86$ (3H, t); ^{13}C NMR (125 MHz, CDCl_3) $\delta = 174.2$; 51.3; 34.2; 32.1; 29.9; 29.8; 29.7; 29.5; 29.4; 29.3; 29.2; 25.1; 22.7; 14.2.

$\text{CH}_3\text{-(CH}_2\text{)}_{14}\text{-COOMe}$: ^1H NMR (500 MHz, CDCl_3) $\delta = 3.71$ (3H, s); $\delta = 2.26\text{--}2.24$ (2H, t); $\delta = 1.60\text{--}1.57$ (2H, m); $\delta = 1.25\text{--}1.22$ (24H, m); $\delta = 0.86$ (3H, t); ^{13}C NMR (125 MHz, CDCl_3) $\delta = 174.5$; 51.5; 34.3; 32.2; 29.9; 29.8; 29.7; 29.6; 29.5; 29.4; 29.3; 25.2; 22.9; 14.3.

$\text{CH}_3\text{-(CH}_2\text{)}_{16}\text{-COOMe}$: ^1H NMR (500 MHz, CDCl_3) $\delta = 3.65$ (3H, s); $\delta = 2.28\text{--}2.25$ (2H, t); $\delta = 1.60\text{--}1.57$ (2H, m); $\delta = 1.25$ (28H, m); $\delta = 0.88$ (3H, t); ^{13}C NMR (125 MHz, CDCl_3) $\delta = 174.6$; 51.4; 34.2; 32.1; 29.8; 29.7; 29.7; 29.6; 29.5; 29.4; 29.3; 25.1; 22.8; 14.2.

$\text{CH}_3\text{(CH}_2\text{)}_7\text{CH=CH(CH}_2\text{)}_7\text{COOMe}$: ^1H NMR (500 MHz, CDCl_3) $\delta = 5.34$ (2H, m); 3.63 (3H, s); 2.29 (2H, t); 2.03-1.95 (4H, m); 1.16-1.56 (2H, m); 1.28-1.23 (20H, m); 0.88 (3H, m); ^{13}C NMR (125 MHz, CDCl_3) $\delta = 174.6$; 130.0; 51.4; 34.2; 32.0; 29.8; 29.7; 29.6; 29.5; 29.4; 29.3; 29.2; 29.1; 27.3; 27.2; 25.7; 25.0; 22.7; 14.1.

$\text{MeOOC-(CH}_2\text{)}_4\text{-COOMe}$: ^1H NMR (500 MHz, CDCl_3) $\delta = 3.65$ (6H, s); $\delta = 2.30\text{--}2.35$ (4H, t); $\delta = 1.59\text{--}1.56$ (4H, m); ^{13}C NMR (125 MHz, CDCl_3) $\delta = 174.7$; 51.5; 33.7; 33.5; 24.4; 24.3; 24.2.

MeOOC-(CH₂)₈-COOMe : ¹H NMR (500 MHz, CDCl₃) δ = 3.66 (6H, s); δ = 2.32-2.25 (4H, t); δ = 1.54-1.51 (4H, m); δ = 1.30 (8H, s); ¹³C NMR (125 MHz, CDCl₃) δ = 174.4; 51.3; 33.9; 28.9; 24.8.

4.9.1. Dependence of catalyst loading

To optimize the utility of Fe@TFMS catalyst for the biodiesel production, the five different sets of esterification reaction has been carried out by varying the catalyst amount from 0 mg to 25 mg at room temperature using 1.0 mmol of lauric acid and 10 mL methanol. From Figure 12, it is quite clear that with the increase in amount of catalyst loading the product yield is increased, maximum up to 97 mol%. But with further increase in catalyst amount in reaction mixture, no significant change is observed in product yield. So, 20 mg catalyst is the best quantity for biodiesel synthesis using 1 mmol of lauric acid for 12 h at room temperature.

4.9.2. Catalyst dependent experiment

To carry out the control experiment 1.0 mmol of lauric acid and 10 mL methanol were taken as a representative example. It has been observed from table 2 that no esterified product was formed in absence of any catalyst at room temperature whereas 7% product yield was obtained without any catalyst by raising the temperature at 65 °C. We have also performed the same reaction using TFMS at two different temperatures, varying the reaction time duration. However, in this case no desired product was formed, the starting compound remains unchanged. Due to these unsatisfactory results the reaction was carried out using other two catalysts like anhydrous FeCl₃ and Fe₃O₄. In the first case the product yield is 47% coming from lewis acidic site but due to their homogeneous nature the catalyst is not reusable furthermore. In second case the product yield was found to be 32% at room temperature as because there was no surface area. But using Fe@TFMS catalyst the biodiesel product yield

was very high (97%) due to high surface area which facilitates the reactant molecule to enter into the pore and come in close proximity to the acid active site of the material. This experimental result surely proves that the high surface area and porosity have crucial roles for production of biodiesel from free fatty acid at room temperature.

4.9.3. Catalyst life time study

Magnetic separation is very simple and interesting technique, and also it can prevent any loss of catalyst during recollection which also helps to increase the recycling ability. After the reaction, when the stirring is stopped the Fe@TFMS nanocatalyst became stuck onto the magnetic stirring bar due to their superparamagnetic behaviour. To check the reusability of the material, the catalyst was repeatedly washed with methanol and acetone to get rid of very trace amount of unreacted free long chain fatty acid. The catalyst is reused for same reaction, after drying it in 75 °C oven for 24 h where lauric acid is chosen as a model example. The recycling efficiency of the catalyst for five consecutive reactions has been shown in Figure 13. It confirms that the Fe@TFMS catalyst can be reused for five reaction cycle without any loss of catalytic activity. Then the reused catalysis is further characterized through PXRD pattern, which suggest that the parent mesoporous structure and characteristic sharp peak for Fe₃O₄ nanocrystals have been retained.

4.9.4. Heterogeneity test

In order to investigate the characteristic nature and also to examine the source of catalytic activity of Fe@TFMS nanocatalyst, we have performed the leaching test experiment. At first, the catalyst is isolated from the reaction mixture by simple magnetically separation technique. Then, after addition of nitric acid solution (30 wt %) to the filtrate, the solution is adjusted to 5 wt % nitric acid solution. The Fe content filtrate solution is analyzed by atomic absorption spectrometric (AAS) analysis. The absence of iron in the filtrate

solution suggested no leaching of Fe from the catalyst surface and solution remains colourless. The experimental analysis clearly signifies that Fe₃O₄ NPs are bound strongly with the thiol functionalized mesoporous MCM-41 and the Fe@TFMS catalyst is heterogeneous in nature.

5. Conclusion

We can conclude that magnetically recoverable heterogeneous Lewis acid catalyst Fe₃O₄ can be immobilized very efficiently over the thiol functionalized 2D-hexagonal mesoporous silica material. Resulting nanomaterial have considerably high surface area of 411 m²g⁻¹ and this material is successfully employed for the biodiesel production from various long chain fatty acids and soybean oil as a vegetable oil under very mild and eco-friendly conditions. Due to superparamagnetic nature of the Fe₃O₄ immobilized nanocatalyst, it is very easy to separate the catalyst from the reaction mixture and it displays high recycling efficiency. Thus, Fe₃O₄ immobilized mesoporous nanocatalyst has open new opportunities for the synthesis of biodiesels in larger scale.

Acknowledgement

PB wishes to thank CSIR, New Delhi for Junior Research Fellowships. Authors wishes to thank DST, New Delhi and British Council, UK for financial supports through the UKIERI project grant (IND/Cont (E) 14-15/055).

References

- [1] D. E. Lopez, J. G. Goodwin, D. A. Bruce, S. Furuta, *Appl. Catal. A: Gen.* 339 (2008) 76-83.
- [2] C. Pirola, F. Galli, C. L. Bianchi, D. C. Boffito, A. Comazzi, F. Manenti, *Energy Fuels* 28 (2014) 5236-5240.
- [3] R. Luque, J. H. Clark, *ChemCatChem.* 3 (2011) 594-597.
- [4] P. S. Sreeprasanth, R. Srivastava, D. Srinivas, P. Ratnasamy. *Appl. Catal. A: Gen.* 314 (2006) 148-159.
- [5] C. Pirola, F. Galli, C. L. Bianchi, D. C. Boffito, A. Comazzi, F. Manenti, *Energy Fuels* 28 (2014) 5236-5240.
- [6] R. Chakraborty, H. Sahu, *Appl. Energy* 114 (2014) 827-836.
- [7] Zillillah, G. Tan, Z. Li, *Green Chem.* 14 (2012) 3077-3086.
- [8] A. Karmakar, M. F. C. G. da Silva, A. J. L. Pombeiro, *Dalton Trans.* 43 (2014) 7795-7810.
- [9] B. Ye, F. Qiu, C. Sun, Y. Li, D. Yang, *Chem. Eng. Technol.* 37 (2014) 283–292.
- [10] J. Fu, L. Chen, P. Lv, L. Yang, Z. Yuan, *Fuel* 154 (2015) 1-8.
- [11] B. He, Y. Shao, Y. Ren, J. Li, Y. Cheng, *Fuel Process. Technol.* 130 (2015) 1-6.
- [12] Y. Zhang, M. Stanciulescu, M. Ikura, *Appl. Catal. A* 366 (2009) 176-183.
- [13] L. Zatta, E. J. M. Paiva, M. L. Corazza, F. Wypych, L. P. Ramos, *Energy Fuels* 28 (2014) 5834-5840.
- [14] S. Y. Chen, T. Yokoi, C. Y. Tang, L. Y. Jang, T. Tatsumi, J. C. C. Chan, S. F. Cheng, *Green Chem.* 13 (2011) 2920-2930.
- [15] D. Zareyee, M. Serehneh, *J. Mol. Catal. A: Chem.* 391 (2014) 88-91.
- [16] T. Sen, I. J. Bruce, T. Mercer, *Chem. Commun.* 46 (2010) 6807-6809.

- [17] S. S. Vieira, Z. M. Magriotisa, M. F. Ribeiro, I. Graçab, A. Fernandesb, J. M. F. M. Lopesb, S. M. Coelhoa, N. A. V. Santosa, A. A. Saczk, *Microporous Mesoporous Mater.* 201 (2015) 160-168.
- [18] D. E. López, J. G. Goodwin Jr., D. A. Bruce, E. Lotero, *Appl. Catal. A* 295 (2005) 97-105.
- [19] A. A. Kiss, A. C. Dimian, G. Rothenberg, *Energy Fuels* 22 (2008) 598-604.
- [20] X. R. Chen, Y. H. Ju, C. Y. Mou, *J. Phys. Chem. C* 111 (2007) 18731-18737.
- [21] N. A. Zafiroopoulos, H. L. Ngo, T. A. Foglia, E. T. Samulski, W. Lin, *Chem. Commun.* 35 (2007) 3670-3672.
- [22] F. Su, Y. Guo, *Green Chem.* 16 (2014) 2934-2957.
- [23] N. Pal, E. B. Cho, D. Kim, M. Jaroniec, *J. Phys. Chem. C* 118 (2014) 15892-15901.
- [24] G. M. Ziarani, N. Lashgari, A. Badiiei, *J. Mol. Catal. A: Chem.* 397 (2015) 166-191.
- [25] H. Wan, C. Chen, Z. Wu, Y. Que, Y. Feng, W. Wang, L. Wang, G. Guan, X. Liu. *ChemCatChem* 7 (2015) 441-449.
- [26] M. Pramanik, M. Nandi, H. Uyama, A. Bhaumik, *Green Chem.* 14 (2012) 2273–2281.
- [27] F. G. Cirujano, A. Corma, F. X. L. I. Xamena, *Chem. Eng. Sci.* 124 (2015) 52-60.
- [28] L. He, S. Qin, T. Chang, Y. Suna, X. Gao, *Catal. Sci. Technol.* 3 (2013) 1102-1107.
- [29] F. Liu, S. Zuo, W. Kong C. Qi, *Green Chem.* 14 (2012) 1342-1349.
- [30] D. Fang, J. Yang, C. Jiao, *ACS Catal.* 1 (2011) 42-47.
- [31] Z. Bi, B. B. He, A. G. McDonald, *Energy Fuels* 29 (2015) 5018-5027.
- [32] W. Thitsartarn, S. Kawi, *Green Chem.* 13 (2011) 3423-3430.
- [33] K. Y. Nandiwale, V. V. Bokade. *Environ. Prog. Sustain. J.* 34 (2015) 795-801.
- [34] S. Bhunia, B. Banerjee, A. Bhaumik, *Chem. Commun.* 51 (2015) 5020-5023.
- [35] S. Tang, L. Wang, Y. Zhang, S. Li, S. Tian, B. Wang, *Fuel Process. Technol.* 95 (2012), 84-89.

- [36] H. Wan, Z. Wu, W. Chen, G. Guan, Y. Cai, C. Chen, Z. Li, X. Liu, *J. Mol. Catal. A: Chem.* 398 (2015) 127-132.
- [37] J. J. Morrison, C. J. Love, B. W. Manson, I. J. Shannon, R. E. Morris, *J. Mater. Chem.* 12 (2002) 3208-3212.
- [38] S. K. Kundu, J. Mondal, A. Bhaumik, *Dalton Trans.* 42 (2013) 10515-10524.
- [39] M. Ilibi, T. B. de Queiroz, J. J. Ren, L. De Cola, A. S. S. de Camargo, H. Eckert, *Dalton Trans.* 43 (2014) 8318-8330.
- [40] J. Mondal, T. Sen, A. Bhaumik, *Dalton Trans.* 41 (2012) 6173-6181.
- [41] C. T. Kresge, M. E. Leonowicz, W. J. Roth, J. C. Vartuli, J. S. Beck, *Nature*.359 (1992) 710-712.
- [42] T. Sen, I. J. Bruce, *Microporous Mesoporous Mater.* 120 (2009) 246-251.
- [43] M. E. Sharifabad, B. Hodgson, M. Jellite, T. Mercer, T. Sen, *Chem. Commun.* 50 (2014) 11185-11187.
- [44] M. Muhler, R. Schlögl, G. Ertl, *J. Catal.* 138 (1992) 413-444.
- [45] W. J. Liu, K. Tian, H. Jiang, H. Q. Yu, *Sci. Rep.* 3 (2013) 2419.
- [46] A. Q. Wang, X. Liu, Z. X. Su, H. W. Jing, *Catal. Sci. Technol.* 4 (2014) 71-80.
- [47] M. L. Savaliya, B. Z. Dholakiya, *Appl. Catal. A: Gen.* 494 (2015) 12-21.
- [48] L. Lin, H. Cui, S. Vittayapadung, Z. Xiao, W. Wu, A. Zhang, W. Mamdough, C. Li, *Environ. Prog. Sustain. Energy* 33 (2014) 1432-1437.
- [49] M. Pramanik, A. Bhaumik, *Chem. Eur. J.* 19 (2013) 8507-8514.

Figure Captions

Figure 1. Small angle powder XRD pattern of as synthesized TFMS (a), extracted TFMS (b) and Fe@TFMS sample.

Figure 2. Wide angle powder XRD pattern of Fe@TFMS sample.

Figure 3. N₂ adsorption/desorption isotherm of the mesoporous catalyst Fe@TFMS. Pore size distributions determined by the NLDFT (Non Local Density Functional Theory) method is shown in the inset.

Figure 4. FTIR spectra of Fe@TFMS (a) and TFMS (b) sample.

Figure 5. TGA/DTA curve for Fe@TFMS material.

Figure 6. Magnetisation curve of the Fe@TFMS nanocomposite.

Figure 7. XPS spectrum of Fe 3p (a), Fe 2p (b), S 2p (c) and S 2s(d) from the surface of Fe@TFMS material.

Figure 8. XPS spectrum in full scan for Fe@TFMS material containing different element.

Figure 9. NH₃-TPD profile diagram of Fe@TFMS material.

Figure 10. UHR-TEM images of Fe₃O₄ nanoparticle at high (a) and low resolution (b), whereas (c) and (d) are UHR-TEM images for Fe@TFMS material. FFT pattern is shown in the inset of (e) and SAED pattern in (f).

Figure 11. FE-SEM image of Fe@TFMS sample.

Figure 12. Dependence of methyl ester product yield (mol %) on catalyst loading amount in esterification reaction of 1mmol lauric acid at room temperature, time 12 h.

Figure 13. Recycling ability of the catalyst Fe@TFMS in the esterification of lauric acid.

Scheme 1. Schematic representation for designing Fe₃O₄ nanoparticle grafted thiol-functionalized MCM-41 material (Fe@TFMS) .

Scheme 2. Proposed mechanism for the esterification reaction over Fe@TFMS catalyst.

Figure 1 [Bhanja, Sen and Bhaumik]

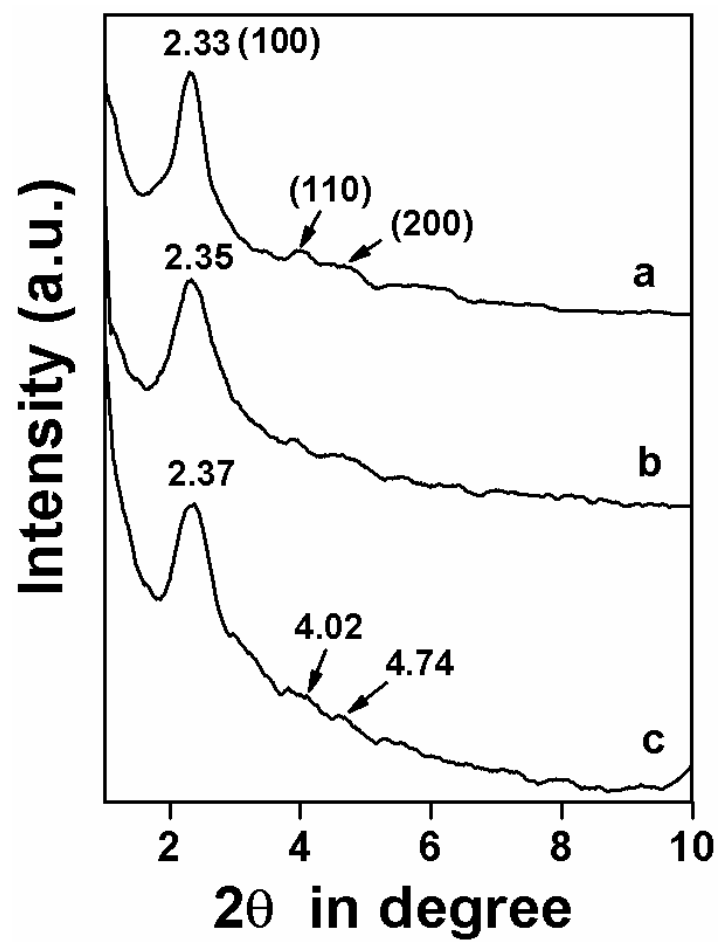


Figure 2 [Bhanja, Sen and Bhaumik]

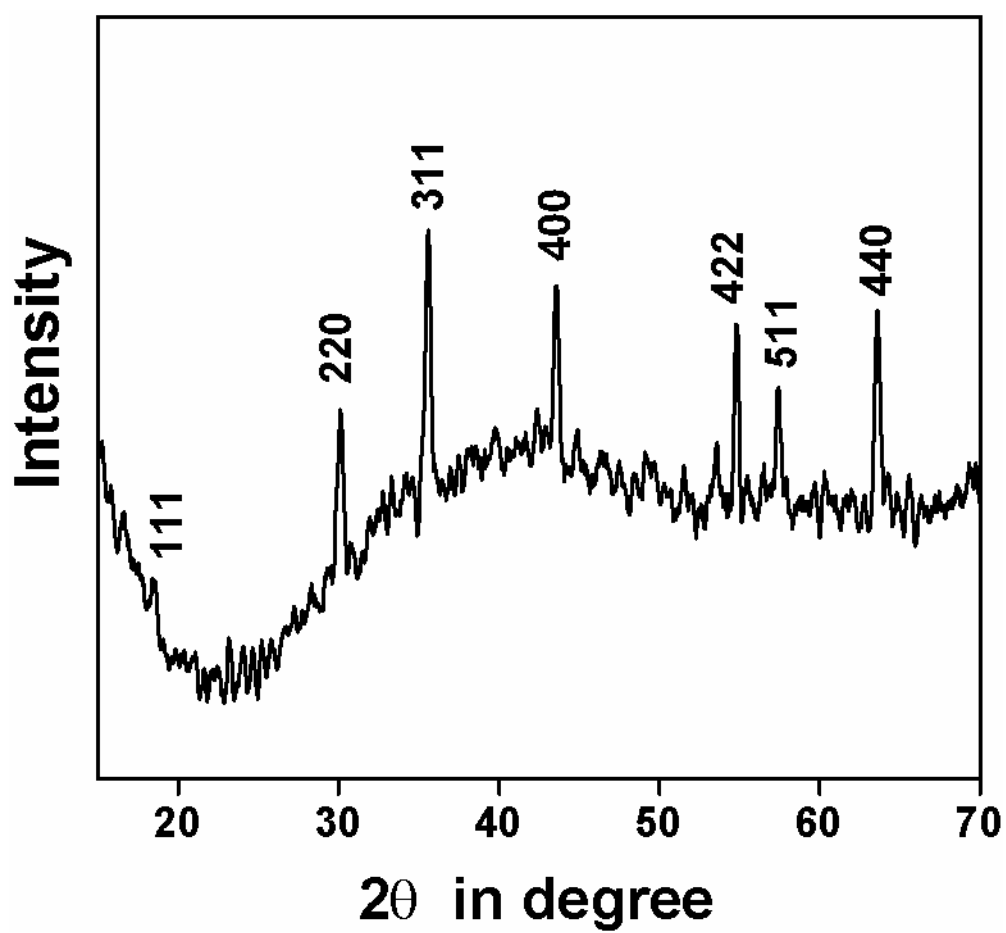


Figure 3 [Bhanja, Sen and Bhaumik]

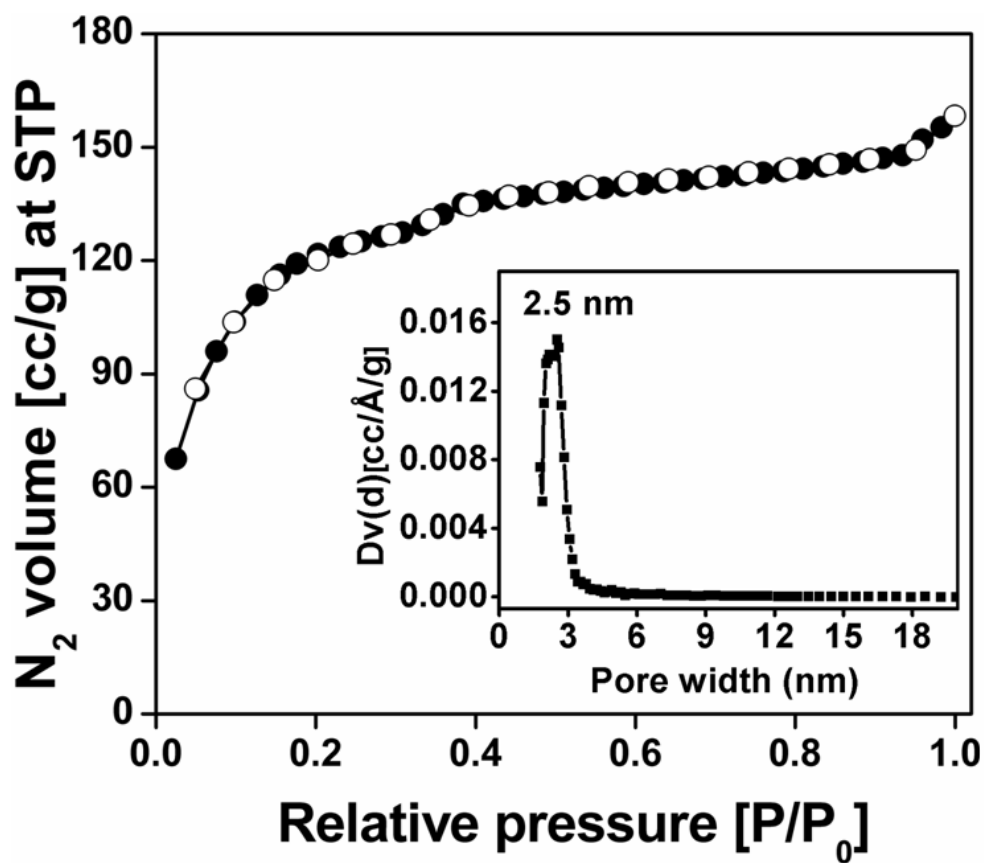


Figure 4 [Bhanja, Sen and Bhaumik]

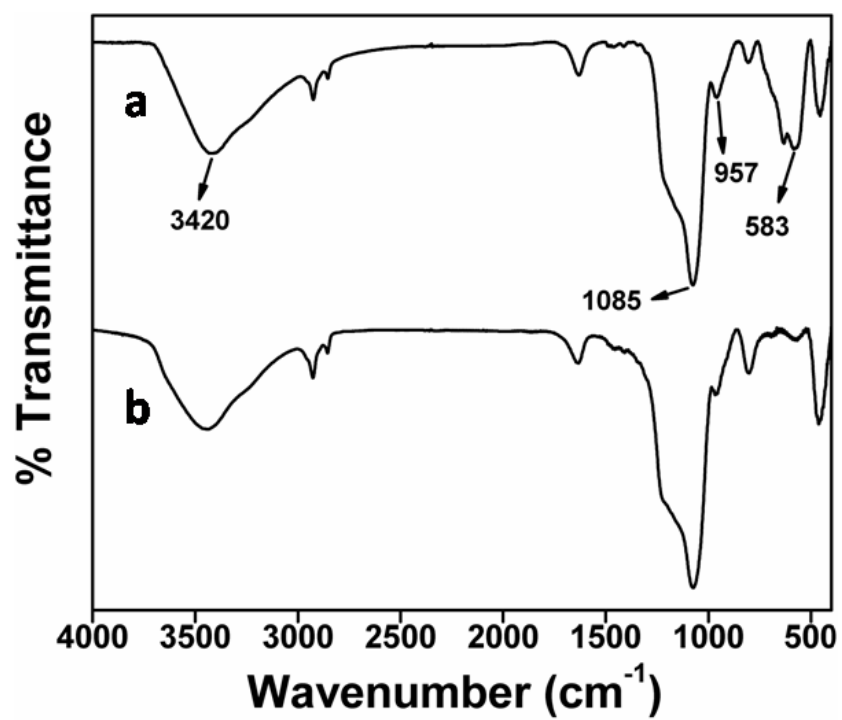


Figure 5 [Bhanja, Sen and Bhaumik]

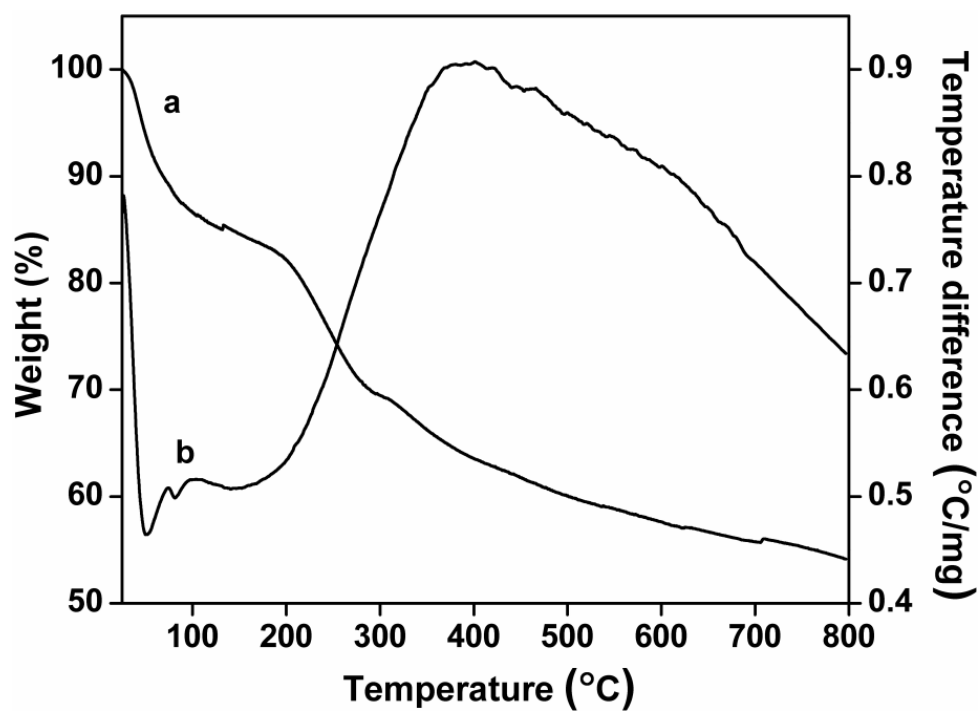


Figure 6 [Bhanja, Sen and Bhaumik]

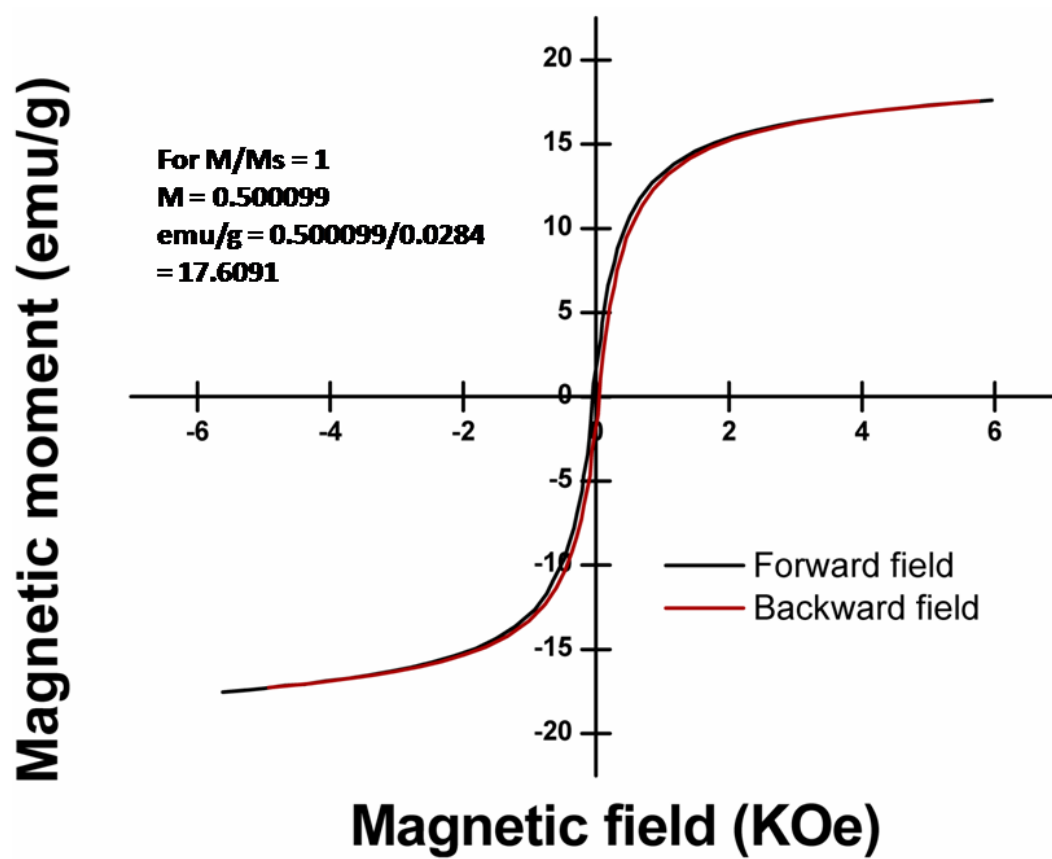


Figure 7 [Bhanja, Sen and Bhaumik]

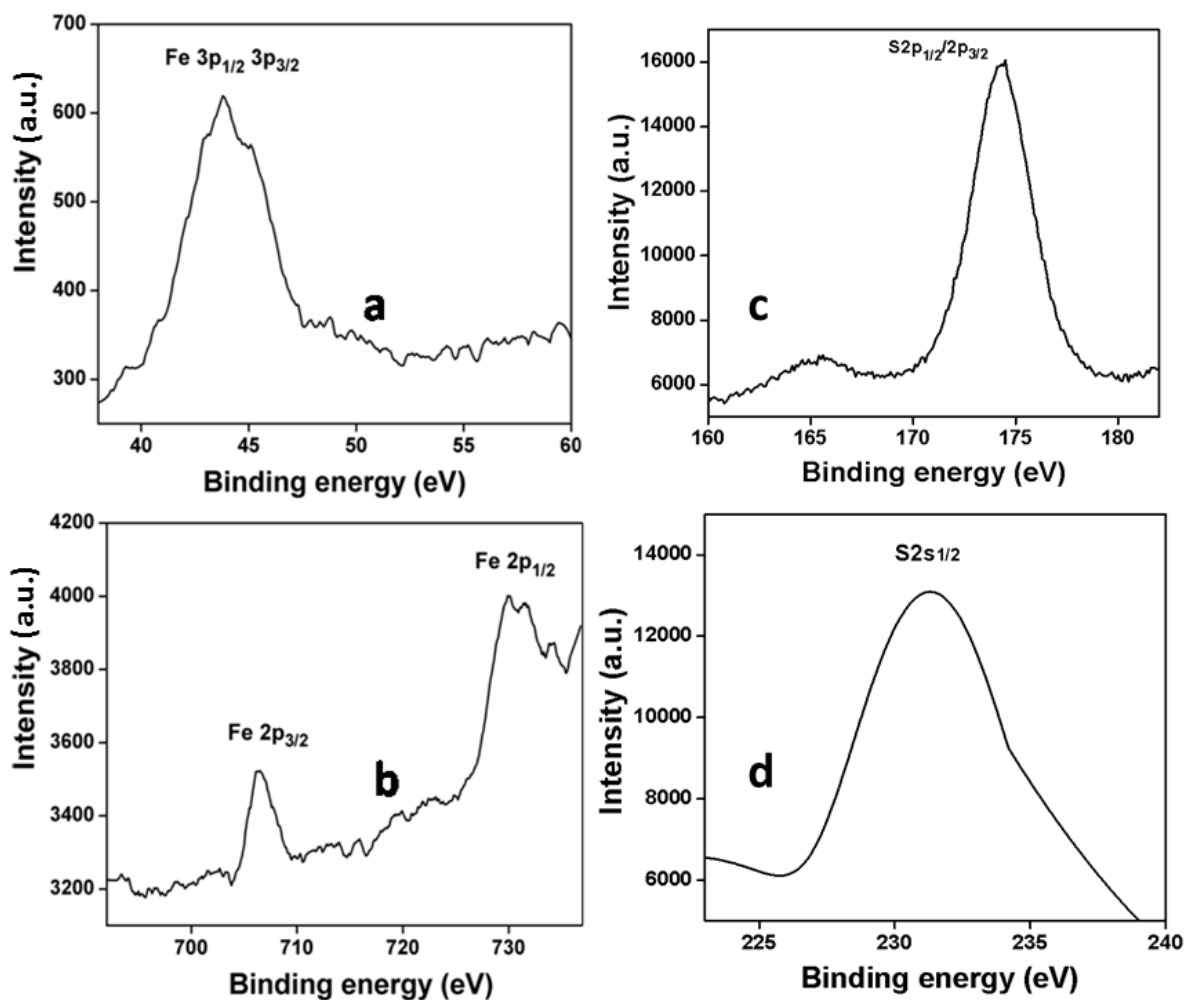


Figure 8 [Bhanja, Sen and Bhaumik]

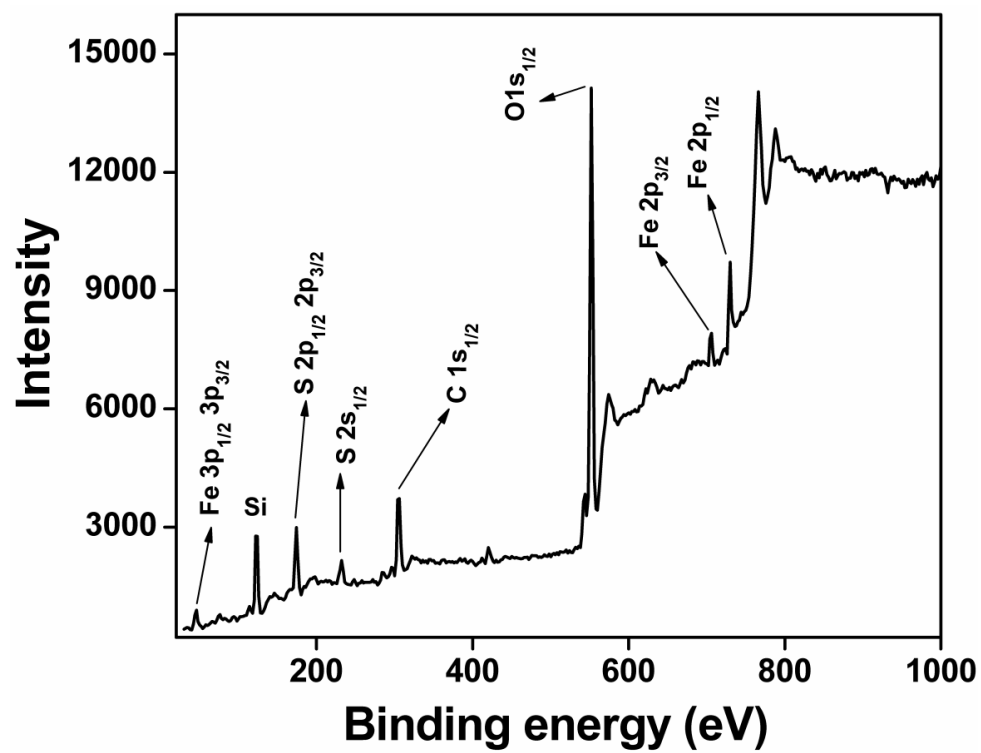


Figure 9 [Bhanja, Sen and Bhaumik]

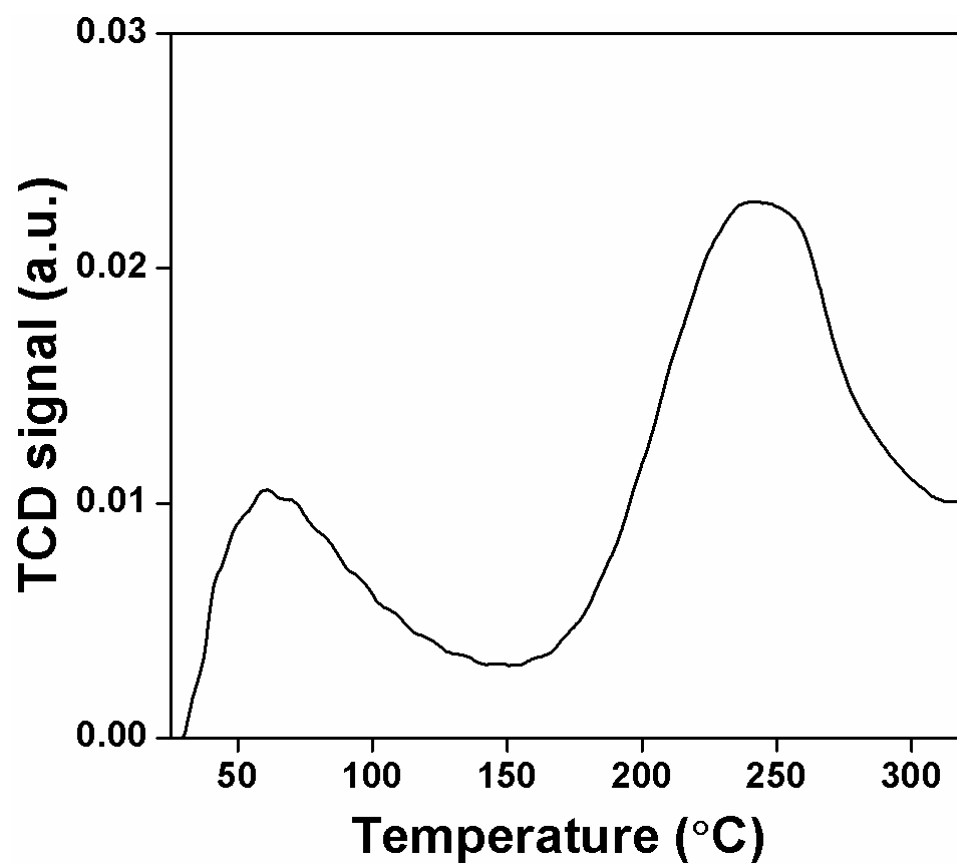


Figure 10 [Bhanja, Sen and Bhaumik]

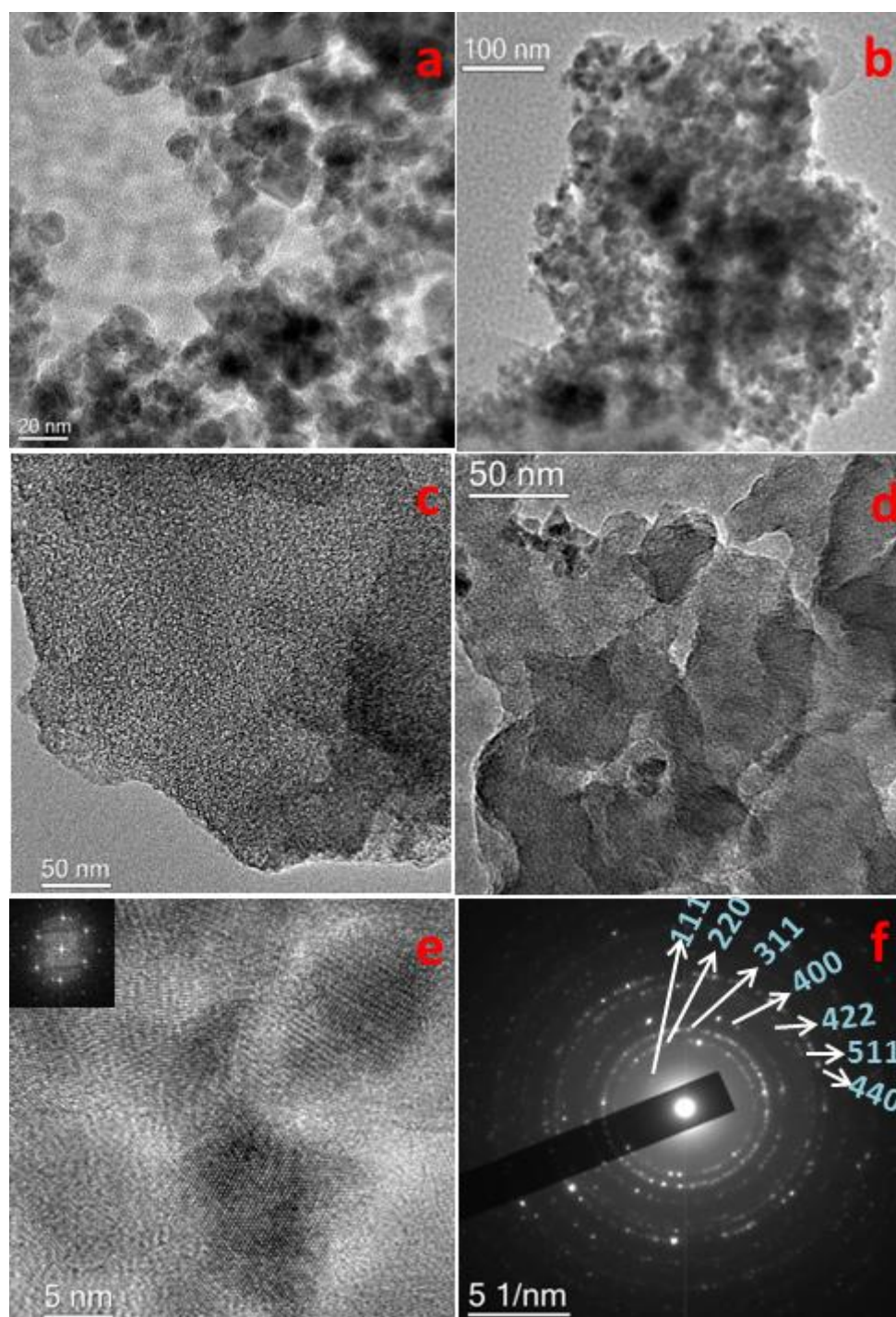


Figure 11 [Bhanja, Sen and Bhaumik]

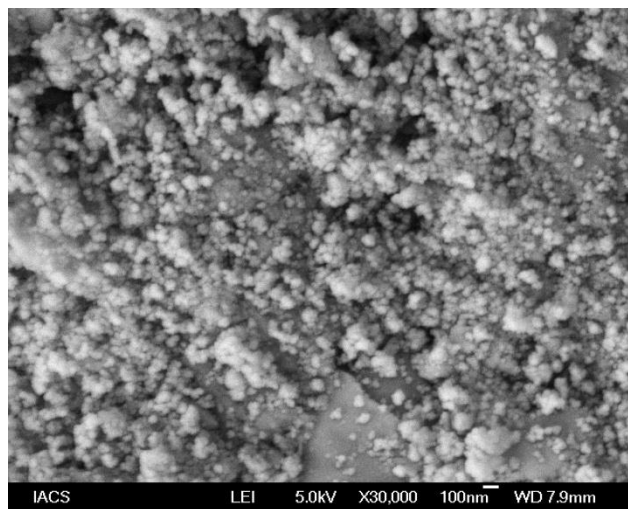


Figure 12[Bhanja, Sen and Bhaumik]

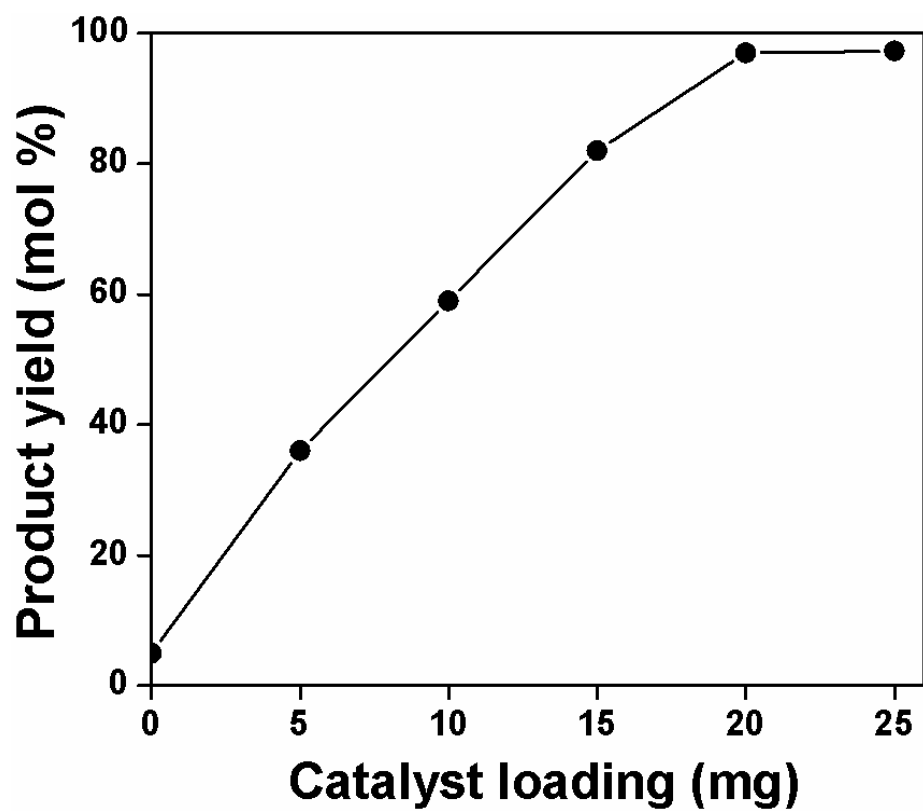
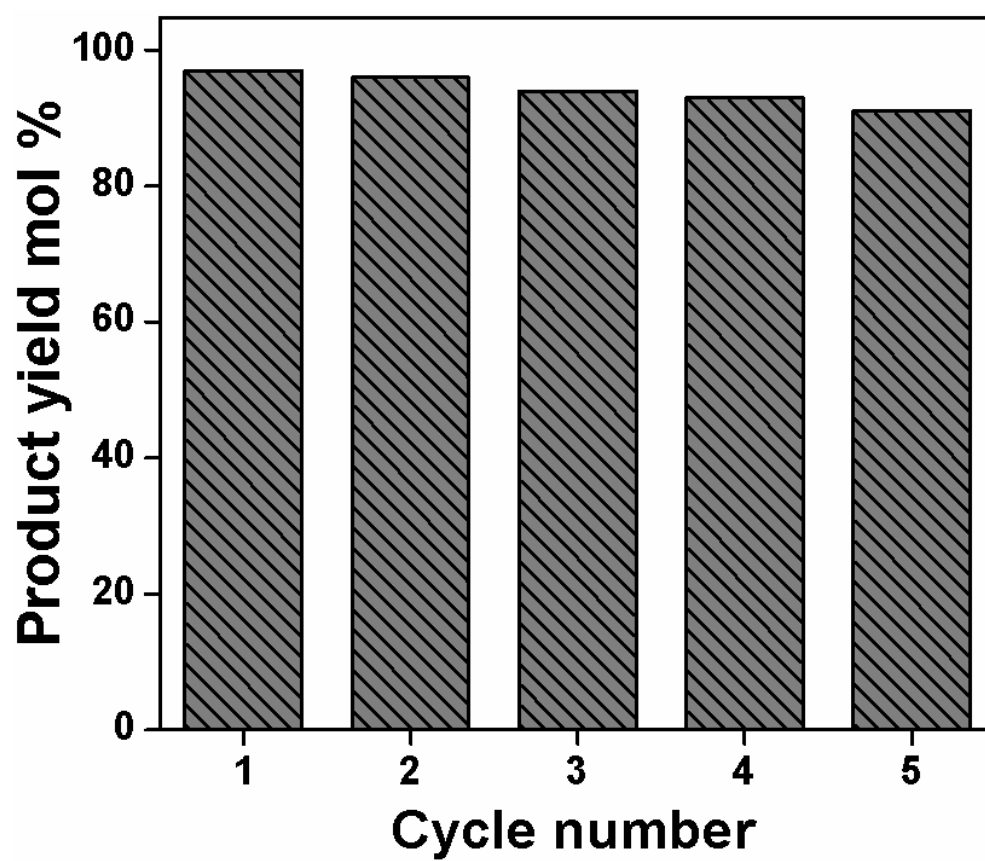
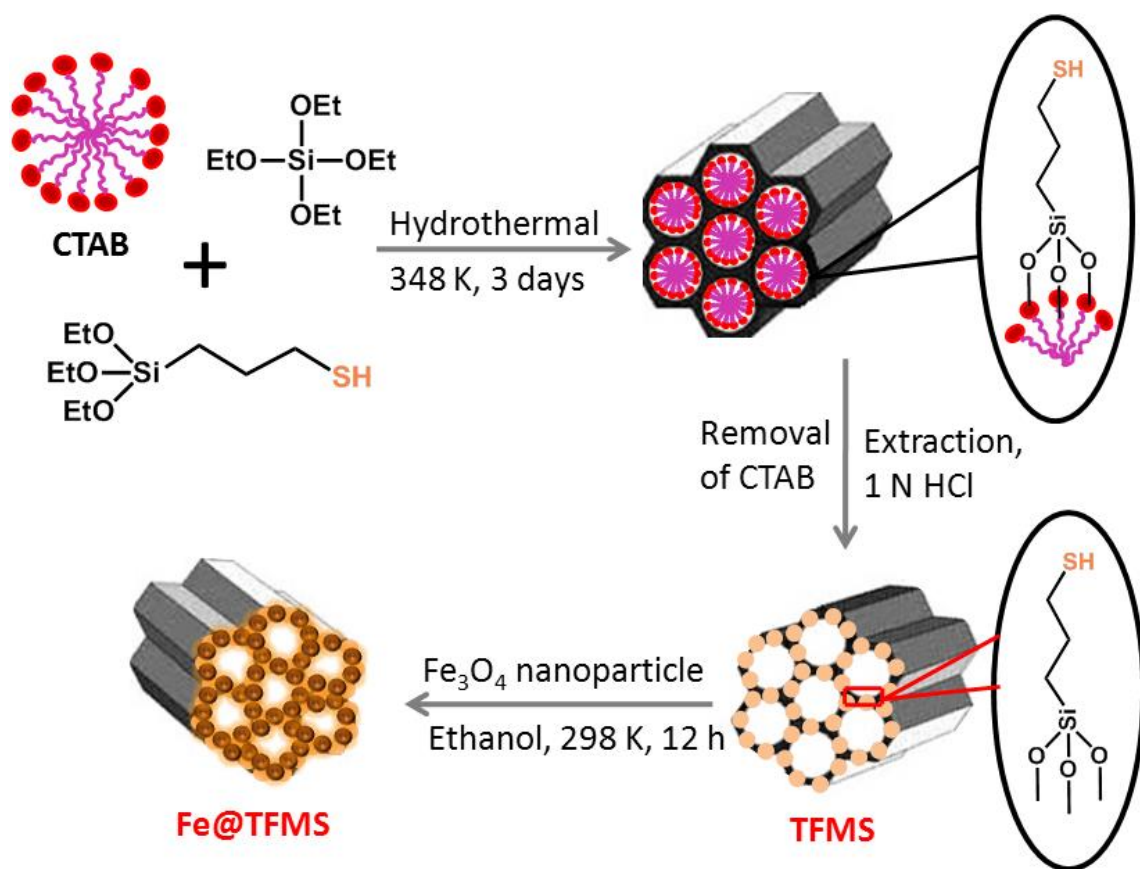


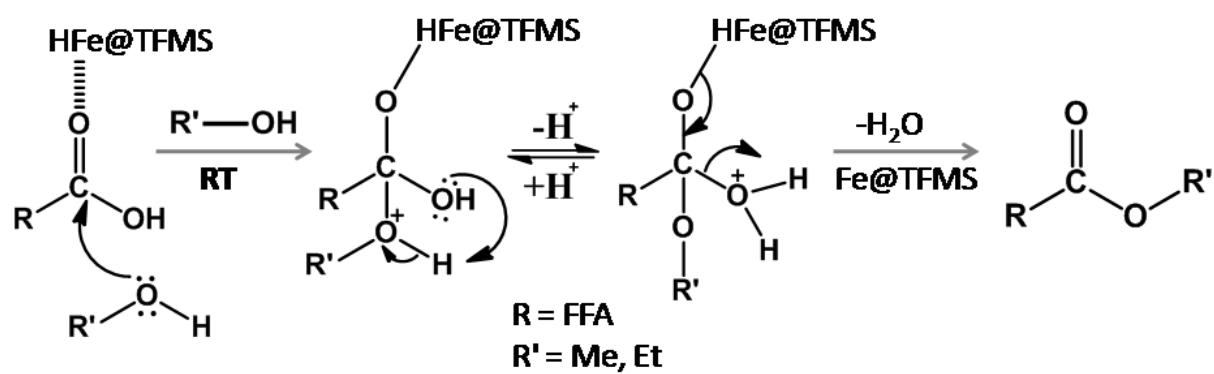
Figure 13 [Bhanja, Sen and Bhaumik]



Scheme 1 [Bhanja, Sen and Bhaumik]



Scheme 2 [Bhanja, Sen and Bhaumik]



Tables

Table 1. Esterification reaction of various long chain fatty acids over Fe@TFMS catalyst

Entry	Fatty acid	Acid : MeOH	Time (h)	Esters of fatty acid	Yield of the product (%)
1	CH ₃ -(CH ₂) ₁₀ -COOMe ^a	1:10	12	CH ₃ -(CH ₂) ₁₀ -COOMe	97
2	CH ₃ -(CH ₂) ₁₂ -COOMe	1:10	12	CH ₃ -(CH ₂) ₁₂ -COOMe	96
3	CH ₃ -(CH ₂) ₁₄ -COOMe	1:10	12	CH ₃ -(CH ₂) ₁₄ -COOMe	97
4	CH ₃ -(CH ₂) ₁₆ -COOMe	1:10	12	CH ₃ -(CH ₂) ₁₆ -COOMe	95
5	CH ₃ (CH ₂) ₇ CH=CH(CH ₂) ₇ COOH	1:10	12	CH ₃ (CH ₂) ₇ CH=CH(CH ₂) ₇ COOMe	93
6	HOOC-(CH ₂) ₄ -COOH ^b	1:20	20	MeOOC-(CH ₂) ₈ -COOMe	95
7	HOOC-(CH ₂) ₈ -COOH	1:20	20	MeOOC-(CH ₂) ₈ -COOMe	96
8	HOOC-(CH ₂) ₄ -COOH ^c	1:20	30	MeOOC-(CH ₂) ₄ -COOMe	7.0

^aReactions are performed using 1mmol fatty acid, 10 mL methanol, 20 mg catalyst loading at room temperature (298 K), for 12 h. Products are identified by ¹H and ¹³C NMR [48].

^bReactions are carried out using 20 mL methanol for 20 h by keeping constant another parameter.

^cYield of the biodiesel product without loading any catalyst in the reaction mixture.

Table 2. Control experiments with various catalysts for biodiesel production.^a

Entry	Catalyst name	Time (h)	Temperature (°C)	Product yield (%)
1.	No catalyst	12	25	0
2.	No catalyst	24	65	7
3.	TFMS	12	25	0
4.	TFMS	24	65	0
5.	Fe@TFMS	12	25	97
6.	Fe ₃ O ₄	12	25	32
7.	Fe ₃ O ₄	24	65	53
8.	FeCl ₃	12	25	47

^aReactions are performed using 1mmol lauric acid, 10 mL methanol, 20 mg catalyst loading at room temperature (298 K).